Computational Materials Science 124 (2016) 220–227

Contents lists available at ScienceDirect

Computational Materials Science

journal homepage: www.elsevier.com/locate/commatsci

# Evaluating the size of Fe nanoparticles for ammonia adsorption and dehydrogenation

G.S. Otero [a], B. Pascucci [a], M.M. Branda [a], R. Miotto [b], P.G. Belelli [a,*]

[a] IFISUR, CONICET and Universidad Nacional del Sur, Av. Alem 1253, 8000 Bahía Blanca, Argentina
[b] Centro de Ciências Naturais e Humanas, Universidade Federal do ABC, Av. Dos Estados 5001, CEP 09210-580, Santo Andre, SP, Brazil

ARTICLE INFO

*Article history:*
Received 22 June 2016
Received in revised form 29 July 2016
Accepted 30 July 2016

*Keywords:*
Nanoclusters
Iron
Ammonia dehydrogenation
DFT

ABSTRACT

The interaction of $NH_3$ with different Fe clusters and nanoparticles was evaluated using a periodic density functional theory method. The preferred adsorption sites, adsorption energies of $NH_3$, the transition states and the corresponding activation energies of the first $NH_3$ dehydrogenation reaction on different small Fe nanoparticles were compared with those obtained for bare Fe(1 1 1) and Fe(1 1 1) with an adatom. On seven clusters investigated ($Fe_{16}$, $Fe_{22}$, $Fe_{32}$, $Fe_{59}$, $Fe_{80}$, $Fe_{113}$ and $Fe_{190}$), $NH_3$ was found to adsorb on top sites, while the $NH_2$ and H products adsorb on bridge and hollow sites, respectively. Higher $NH_3$ adsorption energies were obtained and the dehydrogenation reaction was found to be more exothermic when the size of clusters increases. Although similar activation barriers were found for different nanoparticles and bare surfaces, the $NH_3$ first dehydrogenation is favored when the size of nanoclusters increases.


## 1. Introduction

In the last decade, the new ways to obtain clean hydrogen for proton-exchange in membrane fuel cells (PEMFCs) and other energetic industries have been gaining increased interest, especially for the replacement of natural gas and heating oil [1–4].

Hydrogen is traditionally obtained from gas coal or biomass reforming. However, the new environmental demands indicate the necessity to obtain clean hydrogen, free from carbon residues, through alternative processes. One of these processes has gained noticeable notoriety: the catalytic dehydrogenation of ammonia giving $N_2$ and $H_2$ as final products. Ammonia has some advantages with respect to other conventional hydrogen sources: one is its safe transport and storage as a liquid at relatively low pressures. In addition, liquid ammonia stores 30% more energy than the same amount of liquid hydrogen [1]. Global infrastructure for large-scale production and distribution is already in place.

This potential alternative source of energy has attracted a great deal of attention with the purpose of finding an efficient and economic catalyst to promote $NH_3$ dehydrogenation. Several metallic surfaces, such as Ru, Ni, Fe, Ir, Rh, Pd, Pt and Co [3], have already been tested and proved to be catalysts for ammonia decomposition. Among them, the Ru-based catalyst was found to be the most active at high temperatures (600 K) [5]. However, their high production costs have enabled further developments in order to replace it [4].

In general, these metals are supported to increase dispersion and catalytic stability. Among the most common supports we can mention the $SiO_2$, $Al_2O_3$, $TiO_2$, $ZrO_2$, activated carbon, carbon nanotubes (CNTs) and nanofibers (CNFs) [6–15]. Firstly, the high metal dispersion was designed with a view to increase the number of active sites per available surface area [16]. However, when the particles are extremely small (nanometric size), they show different behavior with respect to systems where extended surfaces are present. This behavior is mainly related to the presence of low coordination sites in nanoparticles, located on edges of steps or corners, improving reactivity significantly. This is consistent with the fact that defects, edges and corners have already been indicated as preferential adsorption sites in a variety of systems ranging from semiconductors to metal surfaces [17–19]. This particular property has been widely explored for different reactions on Fe nanoparticles [20–22].

From the theoretical point of view, the ammonia decomposition has been studied on different close-packed metallic [1,4,23–26] and bimetallic surfaces [5]. From these results, the rate-limiting step of whole reaction cannot be clearly established, since it is extremely dependent on the type of metallic surface [27]. As an example, Duan and co-workers [4,28] and Zhang et al. [8] have recognized the $2N_{ads} \rightarrow N_{2(gas)}$ recombination as the rate determining step of $NH_3$ decomposition; Stolbov and Rahman [1], on the other hand, have indicated that the first dehydrogenation stage needs

* Corresponding author.
*E-mail address:* patricia.belelli@uns.edu.ar (P.G. Belelli).

http://dx.doi.org/10.1016/j.commatsci.2016.07.040
0927-0256/

the highest activation energy ($E_{act}$). Other authors [29–31] have determined by DFT calculations that the hardest step in ammonia dissociation on Fe(1 0 0), Fe(1 0 0) pre-covered with N, and on stepped Fe(2 1 1) is the dehydrogenation from $NH_2$ to NH.

In addition, in order to know the direction of the reaction it is important to be sure that the energetic demand of the first step in the $NH_3$ dissociation will always be lower than the $NH_3$ adsorption energy ($E_{ads}$); in other words, from a thermodynamic point of view, the probability that $NH_3$ dissociation is higher than its desorption [23]. If the ratio $E_{ads}/E_{act}$ is lower than 1, the desorption of $NH_3$ is preferred and the systems do not reach the $2N_{ads} \rightarrow N_{2\,(gas)}$ step. As an example, the energy barrier of the first dehydrogenation on Ni(1 1 1) is higher than $E_{ads}$ by 0.23 eV, thus, the $NH_3$ desorption is more likely to be experimentally observed than its dissociation [1].

Among the most studied transition metals, iron (Fe) was explored because of its availability and low cost. Although its reactivity is smaller than observed for other transition metals, it is expected that it can be enhanced by changing the extended surfaces by nanoparticles [13,32–34]. As it was previously mentioned the shape and size of materials are also important in catalysis, especially when the materials have a size smaller than 10 nm. From the theoretical point of view, Lanzani and Laasonen [35] have used spin-polarized density functional theory to study the bonding and dissociation of $NH_3$ and its fragments on an iron cluster containing 55 atoms. Their results indicated an energy barrier of 1.48 eV for the rate-limiting step, which is associated with the first dehydrogenation; but the dispersion forces were not considered. In a recent work, the dehydrogenation reaction of ammonia was studied on very small iron clusters ($Fe_n$, from n = 1–4) [36], and the results suggest that the hardest step is dependent to the cluster size. The better catalytic activity was found on a monoatomic Fe. In addition Kiss et al. [37], have shown that the properties of small nanoparticles present a molecular character. Therefore, the influence of the nanoparticle size is a key issue in the design of an efficient system for ammonia decomposition.

In this work, the $NH_3$ dissociation on several clusters with different numbers of atoms, from a small cluster of 16 atoms to nanoparticles, up to 190 atoms, was investigated. In order to compare the reactivity of nanoclusters with bare surfaces, the Fe(1 1 1) surface was also analyzed. The most stable sites of $NH_3$ adsorption, their adsorption energies, reaction energies and energy barriers for the first $NH_3$ dehydrogenation on Fe surface and nanoclusters were studied. From these results we could infer the influence of the Fe nanoparticle size in the ammonia dehydrogenation/desorption equilibrium.

## 2. Computational details and models

The calculations corresponding to the ammonia dehydrogenation on iron clusters were performed in the framework of spin-polarized DFT, using the Vienna Ab-Initio Simulation Package (VASP) [38–40]. A cutoff energy of 415 eV gave an accurate convergence for the kinetic energy of plane waves. Increasing the number of special k-points or the basis set results in changes in total energies, atomic distances and vibrational modes that are smaller than 0.1%, 0.2% and 1.0%, respectively. This allows the full convergence of the forces up to $10^{-2}$ eV. The projector augmented wave (PAW) method was used to solve the Kohn-Sham equations [41].

The exchange and correlation effects were described by the generalized gradient approximation (GGA) using the functional expressed by Perdew, Burke and Ernzerhof (PBE) [42]. Since the dispersion effects at the H-metal interaction are not negligible [43] and they are not explicitly considered in the PBE functional, dispersion forces should be addressed in a different way. In this calculation we have used an empirical correction to comprise dispersion forces, as suggested by Grimme [44] and indicated by *disp* for simplicity:

$$E^{DFT-D} = E^{DFT} + E^{disp}$$

where $E^{DFT-D}$ is the total energy of the system, $E^{DFT}$ is the Kohn–Sham total energy as obtained from pure PBE and $E^{disp}$ is an empirical dispersion correction.

For Fe nanoclusters, the numeric integration in the reciprocal space was performed on the gamma point, whereas for surfaces it was carried out on a $5 \times 5 \times 1$ Monkhorst–Pack grid [45].

Iron clusters, $Fe_n$, with n = 16, 22, 32, 59, 80, 113 and 190 atoms were modeled, with an irregular polyhedral structure (Fig. 1). Taking into account that overall, particles with sizes higher than 1 nm are named nanoparticles, and our clusters have diameters between 0.6 nm and 1.6 nm; from now we will write nanoparticles for the three biggest nanoclusters ($Fe_{80}$, $Fe_{113}$ and $Fe_{190}$ with diameter sizes of ~1.1, 1.2 and 1.6 nm, respectively) and clusters for the fourth remaining ones ($Fe_{16}$, $Fe_{22}$, $Fe_{32}$ and $Fe_{59}$). The selection of these nanoclusters is representative; therefore, as the number of atoms increases their dimensions increase likewise. Every cluster was located at the center of a box, maintaining a minimum vacuum region of 10 Å to avoid the interaction with the neighboring nanoparticles, generated by the replication of the unit cell. Before the simulation of $NH_3$ adsorption, the geometries of $Fe_n$ nanoclusters were completely optimized.

Following the studies by Mortensen and co-workers [46], the Fe (1 1 1) surface was represented by a slab containing six atomic layers and the cell used was $(2 \times 2)$. A vacuum region with a thickness greater than 12 Å was included avoiding the interaction between the slabs. In order to study the reactivity of a low coordination Fe atom, a surface containing a Fe adatom was also investigated. It is worth noting that this (1 1 1) plane has Fe atoms at different heights, giving a non-smooth surface appearance. In both cases, the geometry optimization of two uppermost layers was performed.

On the surface and nanoparticle substrates, the adsorption of molecular $NH_3$ and the corresponding fragments of the first dissociation step ($NH_2$ + H) were investigated. In all the substrates, only one $NH_3$ was adsorbed for this reason the coverage on extended surfaces was 0.25 ML.

The $NH_3$ adsorption energies ($E_{ads}$) and the $NH_2$ + H co-adsorption energies ($E_{co\text{-}ads}$) were calculated considering the same reference: the sum of bare substrate and $NH_3$ gas-phase energies (Eqs. (1) and (2)).

$$E_{ads} = E(NH_3/Fe_{surf}) - E(NH_3) - E(Fe_{surf}) \quad (1)$$

$$E_{co\text{-}ads} = E(NH_2 + H/Fe_{surf}) - E(NH_3) - E(Fe_{surf}) \quad (2)$$

Reaction energies ($E_{reac}$) were obtained taking into account the initial (IS) and final states (FS), according to the equation:

$$E_{reac} = E(NH_2 + H/Fe_{surf}) - E(NH_3/Fe_{surf}) \quad (3)$$

where $NH_2$ + $H/Fe_{surf}$ corresponds to both co-adsorbed fragments on Fe surfaces ($Fe_{surf}$) and $NH_3/Fe_{surf}$ to $NH_3$ adsorbed on sustrates.

Transition state geometries (TS) and the activation barriers ($E_{act}$) of reaction were found using the climbing-image Nudged Elastic Band Method (CI-NEB) implemented in VASP [47]. This technique allows finding the minimal energy pathway between the IS and FS states, with the corresponding TS. Through the full vibrational frequency analysis it is possible to assure that the geometry obtained is the saddle point.

The Zero Point energy (ZPE) for $NH_3$, $NH_2$ + H and for transition state energies was analyzed. In agreement with previous calculations [23], no significant differences were found (lower than

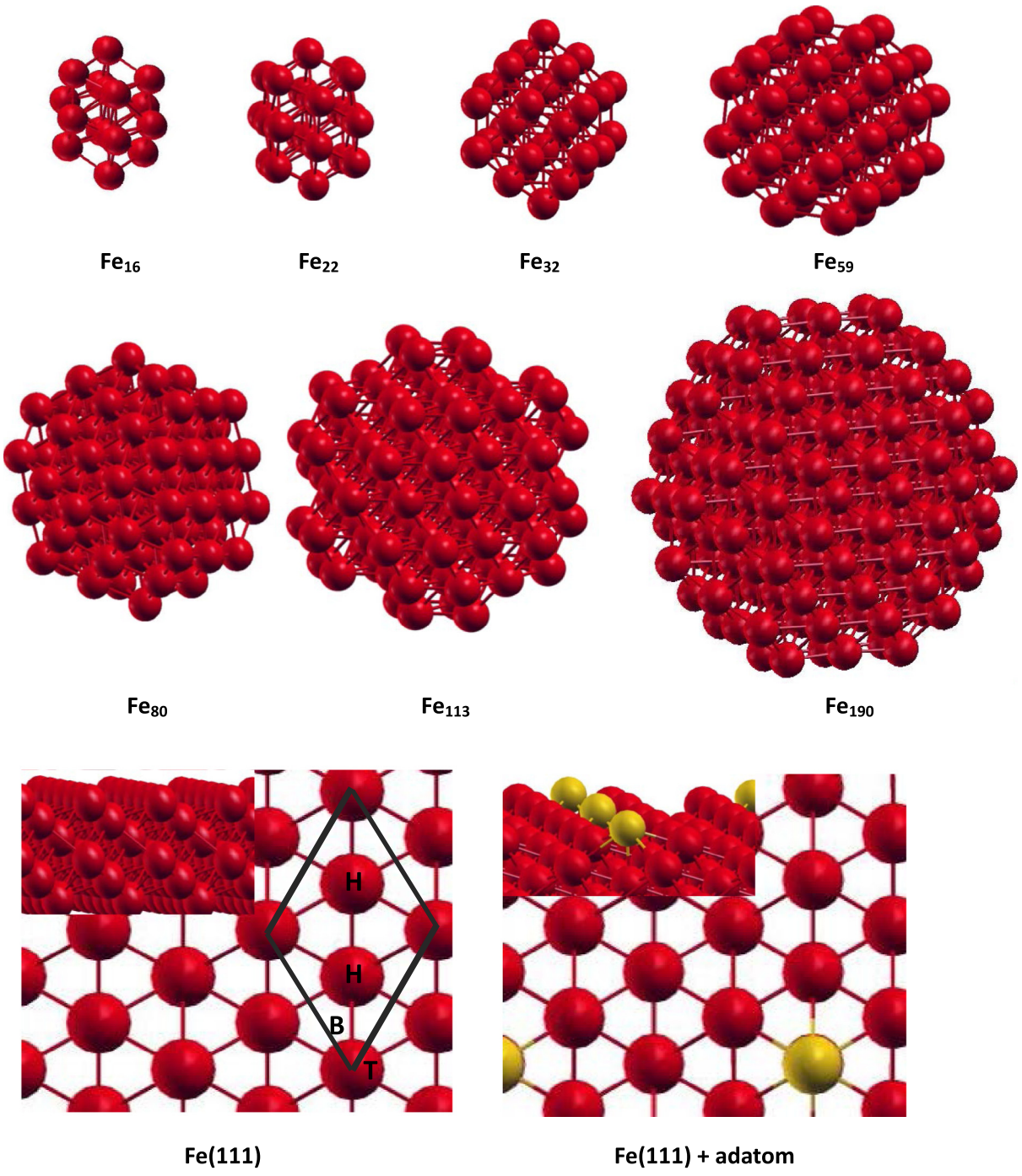


**Fig. 1.** $Fe_n$ nanoclusters, Fe(1 1 1) and Fe(1 1 1) + adatom surfaces. Yellow ball corresponds to adatom. T, B and H correspond to the on-top, bridge and hollow sites, respectively. (For interpretation of the references to color in this figure legend, the reader is referred to the web version of this article.)

0.001 eV). For this reason, it was possible to neglect this correction in our results.

## 3. Results and discussion

### 3.1. Substrate: bare surfaces and nanoparticles

In the first step of our study, we have characterized the bare Fe (1 1 1) surface, the (1 1 1) surface decorated with a Fe adatom, indicated hereafter as Fe(1 1 1) + adatom for simplicity, and different $Fe_n$ nanoclusters. From the geometric point of view, Fe(1 1 1) and Fe(1 1 1) + adatom surfaces are not flat surfaces, but their surface iron atoms are highly coordinated. There are three possible high-symmetry binding sites for Fe adatom on the Fe (1 1 1) surface: on top, twofold bridge and threefold hollow. After geometrical optimization, the most stable position of Fe adatom was found to be at 2.49 Å from three superficial Fe atoms and over a sub-subsurface Fe atom. These bond distances are only slightly longer than on Fe(1 1 1) surface (2.46 Å). This threefold hollow site was also recently reported as the most stable position for an adatom placed onto Fe(1 1 1) surface [48].

An important characteristic of nanoparticles is that each one has different lattice planes exposed upon growth; particularly in the considered cases, (1 1 1) and (1 0 0) planes of fcc

(face-centered cubic) arrangements are found (see Fig. 1). $Fe_{22}$ has four fcc(1 1 1) faces and their corners are connected with two fcc (1 0 0) planes. $Fe_{32}$ is similar to $Fe_{22}$ with more extended surfaces. Although the $Fe_{59}$ structure is comparable with $Fe_{22}$ and $Fe_{32}$ clusters, it has a Fe atom in the center of the cluster.

The increasing number of atoms in the nanoparticles produces larger surface planes for $Fe_{80}$ and $Fe_{190}$ in comparison with smaller clusters. However, the superficial Fe atoms on $Fe_{113}$ have lower coordination numbers than on the previous nanoparticles. Due to this feature it has a more faceted structure.

Taking into account the magnetic character of Fe, the magnetization for both surfaces and all nanoclusters was also analyzed. Our calculated magnetic moments are summarized in Table 1. On the Fe(1 1 1) bare surface, the atomic magnetizations for the surface and subsurface atoms are greater than for the deepest ones. When a Fe adatom is included on Fe(1 1 1) surface, the magnetic arrangement is maintained and the corresponding adatom value is similar to the other superficial atoms. Notwithstanding many investigations of iron surfaces were published, few of them have mentioned the magnetic moment of Fe(1 1 1) surface. Values of 2.62 and 2.81 μB/atom were reported for superficial Fe [49,50]. These values are consistent with the ones calculated in this work, and depicted in Table 1.

The magnetization in nanoclusters increases from the inside to the outer layer, except in $Fe_{32}$, where the greatest magnetization occurs in the subsurface layer (Table 1). The highest magnetization value is located in the furthest atoms from the $Fe_{16}$ cluster center. On the other hand, in $Fe_{59}$ the smallest magnetization value was obtained and corresponds to the central atom in the nanocluster; as it was previously mentioned, this cluster is the only case studied with a single central atom. The outer Fe atoms of nanocluster have the magnetic moment values close to the ones obtained for Fe (1 1 1) surface. Some theoretical works have confirmed that the magnetic moment of Fe clusters is highly influenced by their shapes and sizes, with values between 1.96 and 3.38 μB/atom [51,52]. In agreement with our results, they have found that the smallest cluster $Fe_{13}$ has the highest magnetization value, whereas the larger clusters $Fe_{53}$–$Fe_{57}$ have magnetic values between 1.96 and 2.72 μB/atom.

### 3.2. $NH_3$ adsorption

Different $NH_3$ adsorption sites on Fe(1 1 1), Fe(1 1 1) + adatom surfaces and $Fe_n$ clusters were analyzed. In all cases, ammonia preferentially adsorbs *on-top* sites instead of *bridge* or *hollow* sites, regardless of the iron substrate (Fig. 2). Upon adsorption of the ammonia molecule on Fe(1 1 1), the N atom is bonded to a Fe atom in the on-top configuration and its H atoms are pointing outward from the surfaces, as represented in Fig. 2. In case of Fe(1 1 1) + adatom, $NH_3$ also adsorbs on-top site of the Fe adatom. These results are in complete agreement with those found by other authors on different substrates [2,4,24,25,29,53–58]. Interestingly, for both the bare and the adatom Fe(1 1 1) surfaces, $NH_3$ preferentially adsorbs on sites of low coordination. Except for $Fe_{190}$, the $NH_3$ always adsorbs on an atom in the corner of the nanoparticle, i.e. in a low coordination site. The N—Fe distance is shorter on Fe (1 1 1) surfaces than on nanoparticles and the H—N—H angles are slightly distorted on all substrates, with respect to the corresponding angle in the gas phase $NH_3$ molecule (106.4°) (see Table 2). From periodic density functional calculations, Huang et al. [2] found an H—N—H angle of 110.4° when $NH_3$ is adsorbed on Ir (1 0 0) at 0.25 ML.

We next compare the adsorption energies calculated for the interaction of $NH_3$ with the structures studied. As stated before, the $NH_3$ adsorption energies are similar on Fe(1 1 1) + adatom and on Fe(1 1 1) surfaces, possibly due to the fact that in both cases the molecule adsorbs on Fe atoms with the same coordination number. Our calculated values (~1.1 eV) are higher than those obtained by Satoh et al. [26] (0.94 eV) and Lin et al. [25] (~0.70 eV). We can state at least two reasons for these differences: both authors have used different theoretical approaches and they have not considered dispersion forces in their results. As recently reported by Lejaeghere et al. [59], the use of different codes will inevitably cause variations in the results of the total energy reported. The influence of dispersion forces was also found to be a key issue in the understanding of possible interaction patterns in surfaces, as reported by Schmidt and co-workers [60].

Our theoretical calculations indicate that the adsorption energies increase with the size of the nanocluster. For the $Fe_{80}$ the adsorption energy is already similar to the one obtained for the bare and adatom Fe(1 1 1) surfaces. For larger nanoparticles, the adsorption energy is even larger. Although some oscillations in the adsorption energy values are observed, between $Fe_{32}$ at $Fe_{80}$, there is a clear tendency indicating greater stability of the $NH_3$ adsorbed on larger nanoparticles than on smaller ones.

The interaction between $NH_3$ and Fe nanoparticles was little explored from the theoretical point of view. In the same way as our results, on a top site of small $Fe_n$ clusters, with n = 1–4 atoms, the $NH_3$ adsorption energies increase with the number of Fe atoms, from −0.90 to −1.35 eV for Fe to $Fe_4$, respectively [36].

On the other hand, ammonia adsorption energy of −0.37 eV on a top site of icosahedral $Fe_{55}$ nanocluster was reported by Lanzani and Laasonen [35]. Again the differences observed can be attributed to the use of different theoretical approaches and the inclusion of dispersion forces. Upon adsorption of $NH_3$ on different Fe substrates, the calculated magnetic moments remain almost unchanged, except the Fe(1 1 1) + adatom, where the Fe adatom acquires a negative magnetic moment (changes its spin) (Table 1).

**Table 1**
Magnetic moments (μB/at) of Fe atoms in $Fe_n$ nanoclusters and Fe(1 1 1) surfaces with and without $NH_3$ adsorption and their first dissociation fragments ($NH_2$ + H). For each case, the lower and higher values are presented.

| Magnetic moments | Bare | $NH_3$ | $NH_2$ + H |
|---|---|---|---|
| $Fe_{16}$ | 2.29–3.08 | 2.27–3.13 | 2.41–3.20 |
| $Fe_{22}$ | 2.30–2.83 | 2.27–2.90 | 2.29–2.89 |
| $Fe_{32}$ | 1.93–2.91 | 1.95–2.92 | 1.92–2.95 |
| $Fe_{59}$ | 1.55–2.78 | 1.56–2.81 | 1.58–2.81 |
| $Fe_{80}$ | 2.13–2.89 | 2.14–2.90 | 2.12–2.90 |
| $Fe_{113}$ | 2.16–2.97 | 2.15–2.94 | 1.72–2.92 |
| $Fe_{190}$ | 1.89–2.84 | 1.88–2.85 | 1.89–2.83 |
| Fe(1 1 1) | 2.47–2.91 | 2.44–2.91 | 2.30–2.91 |
| Fe(1 1 1) + adatom[a] | 2.46–2.95 (2.87) | 2.28–2.91 (−2.53) | 2.48–2.94 (2.63) |

[a] In parenthesis the magnetic moment of Fe adatom.

### 3.3. $NH_2$ + H co-adsorption on surfaces and nanoparticles

In the next step of our study, we evaluate the co-adsorption of $NH_2$ and H fragments on the considered substrates, Fe(1 1 1) surfaces and $Fe_n$ clusters, which will allow us to obtain the reaction pathways for the first $NH_3$ dehydrogenation. On Fe(1 1 1) surface, both products are adsorbed on pseudo-bridge sites (Fig. 3). On Fe (1 1 1) + adatom, the products —$NH_2$ and H fragments, also adsorb on bridge sites but the distances are shorter than on Fe(1 1 1) surface (see Table 3). The more favorable sites for the co-adsorption on nanoclusters are slightly different compared with the surfaces. On larger nanoparticles, $NH_2$ and H preferentially adsorb on bridge and hollow sites, respectively (Fig. 3); meanwhile, on small clusters the fragments adsorb on sites of low coordination number. For example on $Fe_{16}$, the more favorable sites for $NH_2$ and H are on top and on bridge sites, respectively; on $Fe_{22}$, both $NH_2$ and H,

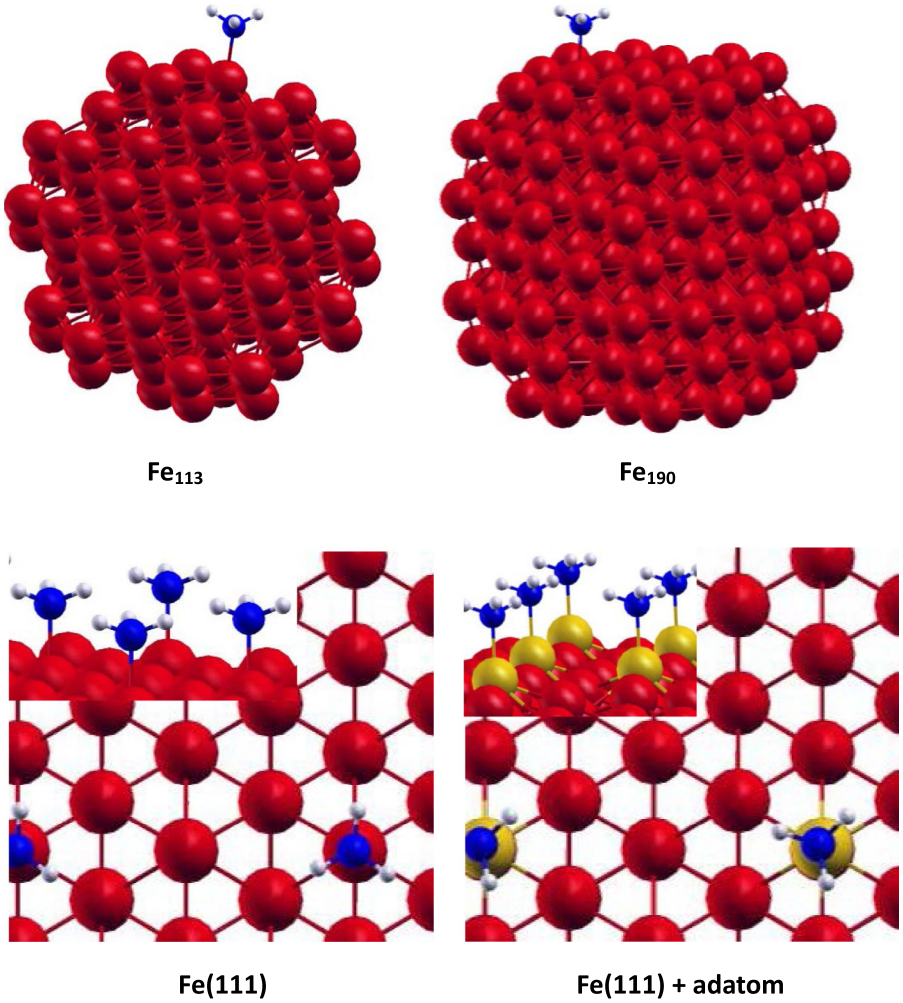


**Fig. 2.** $NH_3$ optimized adsorption geometries on some $Fe_n$ nanoparticles, Fe(1 1 1) and Fe(1 1 1) + adatom surfaces.

**Table 2**
$NH_3$ adsorption energies ($E_{ads}$, eV), N—Fe distances (Å) and H—N—H angles (°) on $Fe_n$ nanoclusters and Fe(1 1 1) surfaces.

| Substrate | $E_{ads}$ | d(N—Fe) | ∠H—N—H |
|---|---|---|---|
| $Fe_{16}$ | −0.96 | 2.13 | 107.3 |
| $Fe_{22}$ | −1.04 | 2.10 | 108.0 |
| $Fe_{32}$ | −0.98 | 2.09 | 107.6 |
| $Fe_{59}$ | −1.01 | 2.10 | 108.0 |
| $Fe_{80}$ | −1.09 | 2.09 | 107.8 |
| $Fe_{113}$ | −1.37 | 2.10 | 107.5 |
| $Fe_{190}$ | −1.59 | 2.14 | 107.1 |
| Fe(1 1 1) | −1.13 | 2.07 | 109.3 |
| Fe(1 1 1) + adatom | −1.10 | 2.10 | 108.1 |

preferentially on bridge sites. For the $Fe_{113}$, $NH_2$ adsorbs specially on a pseudo-bridge site and H on a much lengthened bridge site; it is worth noting that $Fe_{113}$ has a surface with very poor plane development. On the $Fe_{190}$ nanoparticle, the $NH_2$ fragment is located on a bridge site of the (1 1 1) surface, close to an edge. Hydrogen atom migrates to the edge of the surface, far from the $NH_2$ fragment on a pseudo bridge site (3.62 Å). Several authors have reported the $NH_2$ and H co-adsorption on Fe surfaces. Our results for the $NH_2$ and H co-adsorption on Fe(1 1 1), Fe(1 1 1) + adatom surfaces and also on larger nanoparticles with more extended planes are in general agreement with the data reported by other groups [1,2,4,23–25,53,55,56]. On Fe nanoparticles, similar studies are very scarce in literature. Zhang et al. [36], reported the co-adsorption energies of $NH_2$ + H on small iron clusters ($Fe_n$, n = 1–4), although, the corresponding values were related to H and $NH_2$ as isolated species; for this reason, these values are not comparable with ours. The magnetic moments of Fe atoms on different substrates again do not change significantly after the fragments adsorption (Table 1).

The most relevant geometric parameters and co-adsorption energies ($E_{co\text{-}ads}$) are summarized in Table 3. The N—Fe bonds show the shortest values for the on top adsorption, while the longest bonds are on the pseudo-bridge sites. All the N—H distances are extremely stretched. In general, the energy values display a more favorable $NH_2$ + H co-adsorption on the nanoparticles than on Fe (1 1 1) and Fe(1 1 1) + adatom surfaces. In addition, these values are even larger when sizes of the nanoclusters increase. The reaction energies ($E_{reac}$) are exothermic since in all cases the $NH_2$ + H co-adsorptions are more stable in comparison to the $NH_3$ adsorption, and these energies become more exothermic when the nanoparticles grow (Table 4). Similar trends were obtained on iron clusters [36]. The reaction energies of the two largest nanoparticles are similar. From the foregoing results, one could infer that the activation barriers should decrease with the increasing size of the nanoparticles.

### *3.4. Energy pathways for the first $NH_3$ dehydrogenation on iron surfaces and nanoparticles*

Based on the previous results, we evaluated the reaction path for the first dehydrogenation of $NH_3$ on the substrates already

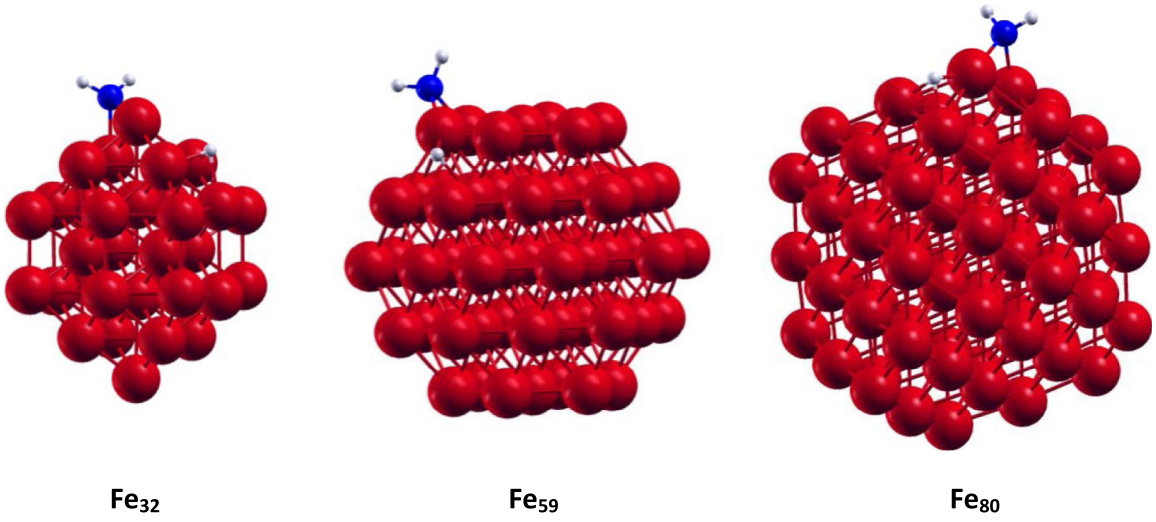


**Fig. 3.** $NH_2$ and H fragments from the first decomposition of $NH_3$ on some $Fe_n$ nanoclusters.

**Table 3**
Co-adsorption energies ($E_{co\text{-}ads}$, eV), N—Fe distances (Å) and H—N—H angles (°) for $NH_2$ + H on $Fe_n$ nanoclusters and Fe(1 1 1) surfaces. The co-adsorption energies were calculated with respect to the $NH_3$ in gas-phase.

| Substrate | $E_{co\text{-}ads}$ | d(N—Fe) | d(N—H) | d(H—Fe) | ∠H—N—H |
|---|---|---|---|---|---|
| $Fe_{16}$ | −0.93 | 1.86 | 3.78 | 1.73 | 109.4 |
| $Fe_{22}$ | −1.41 | 2.00 | 4.38 | 1.72 | 107.9 |
| $Fe_{32}$ | −1.45 | 1.98 | 4.39 | 1.80 | 108.4 |
| $Fe_{59}$ | −1.66 | 1.98 | 3.64 | 1.75 | 108.4 |
| $Fe_{80}$ | −1.92 | 1.97 | 3.54 | 1.78 | 108.4 |
| $Fe_{113}$ | −2.31 | 2.06 | 3.63 | 2.50 | 108.5 |
| $Fe_{190}$ | −2.54 | 2.05 | 3.62 | 2.25 | 108.4 |
| Fe(1 1 1) | −1.41 | 2.01 | 4.11 | 1.71 | 109.3 |
| Fe(1 1 1) + adatom | −1.69 | 1.97 | 3.13 | 1.64 | 108.6 |

**Table 4**
First $NH_3$ dehydrogenation energies ($E_{reac}$, eV) on $Fe_n$ nanoclusters and Fe(1 1 1) surface.

| Substrate | $E_{reac}$ |
|---|---|
| $Fe_{16}$ | 0.03 |
| $Fe_{22}$ | −0.37 |
| $Fe_{32}$ | −0.47 |
| $Fe_{59}$ | −0.65 |
| $Fe_{80}$ | −0.83 |
| $Fe_{113}$ | −0.94 |
| $Fe_{190}$ | −0.95 |
| Fe(1 1 1) | −0.29 |
| Fe(1 1 1) + adatom | −0.59 |

analyzed. Taking into account that the ammonia adsorption energies, $NH_2$ + H co-adsorption energies and the dehydrogenation reaction energies are favored with the increasing size of the nanocluster, we decide to select some of them to study the reaction paths. We choose the Fe(1 1 1) surface and three clusters with different numbers of Fe atoms: $Fe_{22}$, $Fe_{80}$ and $Fe_{113}$. The energy profiles of ammonia dehydrogenation on those substrates are presented in Fig. 4 and the corresponding TS geometries are also included. For this reaction, the activation energies ($E_{act}$) and the more relevant geometric parameters of the transition states on $Fe_n$ nanoclusters and Fe(1 1 1) surface are summarized in Table 5.

The energy profile of the ammonia dehydrogenation on Fe (1 1 1) shows an activation energy of 1.05 eV (see Fig. 4a). This value is slightly lower than the value obtained by Lin et al. [25] on the same surface (1.23 eV). This difference could be attributed to the stronger interaction between adsorbate/substrate calculated with the inclusion of van der Waals correction. On $Fe_{22}$, the reaction occurs with a TS barrier of 1.09 eV (Fig. 4b), very close to the value obtained for the bare Fe(1 1 1) surface. In the other two reaction paths, on $Fe_{80}$ and $Fe_{113}$ nanoparticles, the activation barriers do not differ significantly from the previously discussed values (Fig. 4c and d). Although the activation barriers are similar, the corresponding geometries are different (see Table 5). The N—H distances stretch from a lower value of 1.35 Å to a higher value of 2.69 Å. The largest distance could be attributed to the great variation from the initial to the final geometries, and due to the H position which is near to its final site in the co-adsorption with $NH_2$. Therefore, from a geometric point of view this TS can be considered as a *late TS* (Hammond–Leffler Postulate [61,62]). However, the $NH_2$ fragments in the other cases do not change their positions significantly from the initial $NH_3$ adsorption site, and their TS geometries can be associated with *early* structures, in accordance with the Hammond–Leffler Postulate. As a general trend, these results indicate that the energy required for the first dehydrogenation of $NH_3$ would be associated with the N—H bond rupture instead of the posterior migration of the reaction products to their final sites. The other distances reported do not show significant differences between them.

Taking into account the results obtained one could conclude that the first dehydrogenation reaction of $NH_3$ is strongly related to the substrate (see Fig. 4). On Fe(1 1 1), the activation barrier is slightly lower than the adsorption energy of $NH_3$, indicating that the ammonia desorption will compete with the dehydrogenation. This behavior was also observed for $Fe_{22}$ and $Fe_{80}$: the activation energies and the corresponding adsorption energies have similar values. Finally, the activation barrier on $Fe_{113}$ is lower than the adsorption energy of $NH_3$, for this reason on this nanoparticle the dissociation is promoted. Besides the reverse reaction, the ammonia synthesis, needs the highest activation energy (1.97 eV) on this nanoparticle, compared with other substrates.

The difference between the reactivities of nanoparticles and the extended surfaces is due to the ammonia adsorption and $NH_2$ + H co-adsorption energies. The ammonia dissociation depends on the strength of the $NH_3$ adsorption since the activation energy barriers have similar values for Fe(1 1 1) surface and for all the clusters considered. Despite the fact that the adsorption sites are almost the same on the nanoclusters, the stability of $NH_3$ adsorption increases from the smallest to the largest size. One could infer that the adsorption energy values reach a plateau with increasing nanoparticle size. Taking into account that the reactive sites correspond to edges and

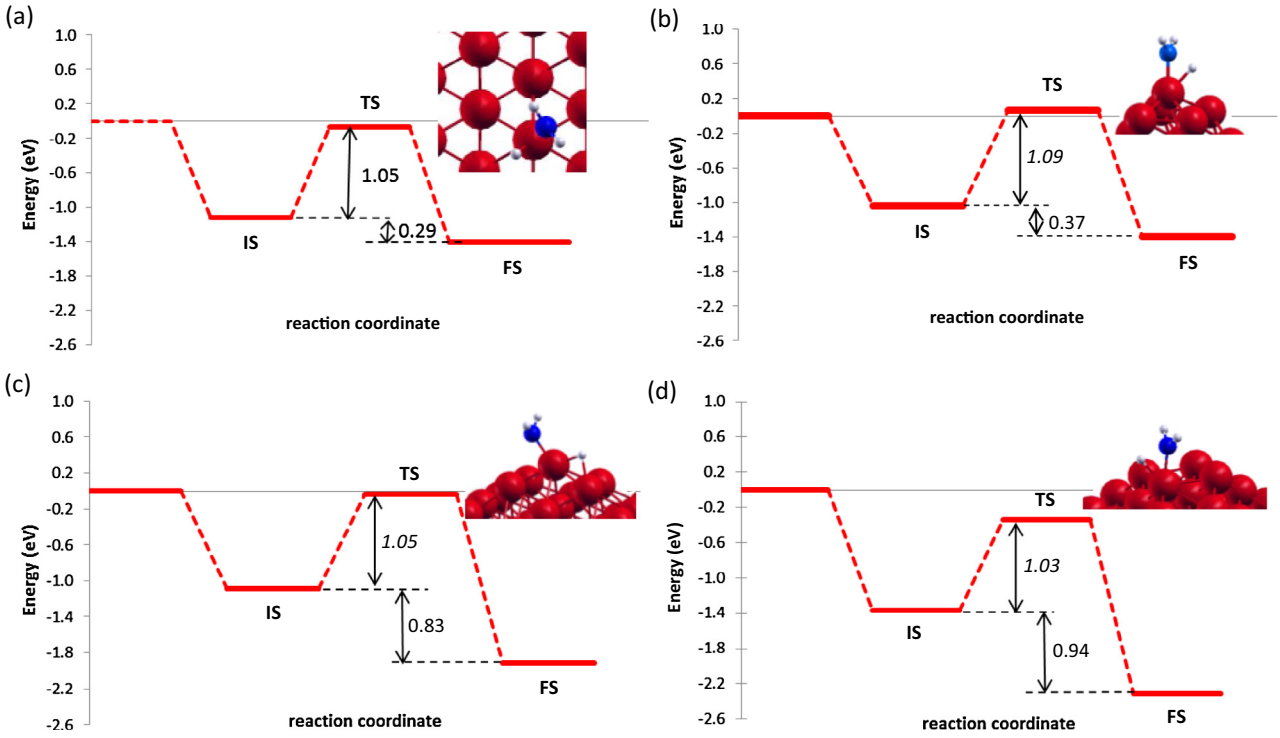


**Fig. 4.** The potential energy profiles and transition state geometries for the first dehydrogenation reaction of $NH_3$ on: (a) Fe(1 1 1); (b) $Fe_{22}$; (c) $Fe_{80}$ and (d) $Fe_{113}$.

**Table 5**
Activation energies ($E_{act}$, eV) and the more relevant geometric parameters (Å) of the transition states for the first $NH_3$ dehydrogenation reaction on $Fe_n$ nanoclusters and Fe(1 1 1) surface.

| Substrate | $E_{act}$ | d(N—Fe) | d(N—H) | d(H—Fe) |
|---|---|---|---|---|
| $Fe_{22}$ | 1.09 | 1.92 | 1.35 | 1.69 |
| $Fe_{80}$ | 1.05 | 1.86 | 2.69 | 1.66 |
| $Fe_{113}$ | 1.03 | 1.85 | 1.40 | 1.71 |
| Fe(1 1 1) | 1.05 | 1.89 | 1.60 | 1.60 |

corners in the nanoparticles studied and that the percentage of these sites decrease with the cluster size, then, it is also expected that the reactivity reverses as soon as the nanoparticle size increases sufficiently. Experimental results of $NH_3$ decomposition on different metal nanoparticles show the higher activities with sizes between 5.0 and 7.0 nm [8,10]. Although our nanoparticle models are smaller, 1.6 nm for $Fe_{190}$, the overall trends are consistent with the experimental observations.

## 4. Conclusions

In this work the stability and the first dehydrogenation reaction of $NH_3$ on nanoclusters with different numbers of atoms and two extended Fe surfaces were evaluated. In all the substrates, the $NH_3$ adsorbs preferentially on-top sites. For the clusters considered in this work, the on-top site is placed in a corner with the exception of the $Fe_{190}$, where it is located in an fcc(1 1 1) plane. The $NH_3$ stability increases for the $Fe_{113}$ and $Fe_{190}$, where the adsorption is clearly stronger than on both Fe(1 1 1) surfaces.

Fragments of the first dissociation reaction ($NH_2 + H$), also increase their stabilities with the increasing size of nanoparticles; consequently the dehydrogenation reaction becomes more exothermic.

On selected clusters and extended Fe(1 1 1) surface, the reaction pathways of the first dehydrogenation of $NH_3$ showed comparable activation barrier values. From these results one could infer that the reaction would depend on the $NH_3$ adsorption strength instead of the activation energy barrier. When the ammonia adsorption is stronger, the dissociation will be promoted rather than the desorption. The dissociation/desorption ratio is favored when the number of atoms forming the nanoparticle is increased.

## Acknowledgements

This research was carried out for the financial support of CONICET – Argentina (PIP 112-2010100949), ANPCyT – Argentina (PICT 2010 - N° 0830) and Universidad Nacional del Sur – Argentina (PGI – UNS N° 24/F051).

## References

[1] S. Stolbov, T.S. Rahman, J. Chem. Phys. 123 (2005). 204716-5.
[2] W. Huang, W. Lai, D. Xie, Surf. Sci. 602 (2008) 1288–1294.
[3] X. Duan, G. Qian, X. Zhou, Z. Sui, D. Chen, W. Yuan, App. Catal. B 101 (2011) 189–196.
[4] X. Duan, J. Ji, G. Qian, C. Fan, Y. Zhu, X. Zhou, D. Chen, W. Yuan, J. Molec. Catal. A: Chem. 357 (2012) 81–86.
[5] D.A. Hangsen, L.M. Thomanek, J.G. Chen, D.G. Vlachos, J. Chem. Phys. 134 (2011). 184701-7.
[6] X.K. Li, W.J. Ji, J. Zhao, S.J. Wang, C.T. Au, J. Catal. 236 (2005) 181–189.
[7] T.V. Choudhary, C. Svadinaragana, D.W. Goodman, Catal. Lett. 72 (2001) 197–201.
[8] J. Zhang, H.Y. Xu, X.L. Jin, Q.J. Ge, W.Z. Li, Appl. Catal. A: Gen. 290 (2005) 87–96.
[9] Y. Liu, H. Wang, J. Li, Y. Lu, Q. Xue, J. Chen, AIChE J. 53 (2007) 1845–1849.
[10] A.M. Karim, V. Prasad, G. Mpourmpakis, W.W. Lonergan, A.I. Frenkel, J.G. Chen, D.G. Vlachos, J. Am. Chem. Soc. 131 (2009) 12230–12239.
[11] S.F. Yin, Q.H. Zhang, B.Q. Xu, W.X. Zhu, C.F. Ng, C.T. Au, J. Catal. 224 (2004) 384–396.
[12] X. Duan, J. Zhou, G. Qian, P. Li, X. Zhou, D. Chen, Chin. J. Catal. 31 (2010) 979–986.
[13] F. Viñes, J.R.B. Gomes, F. Illas, Chem. Soc. Rev. 43 (2014) 4922–4939.
[14] J. Zhang, M. Comotti, F. Schüth, R. Schlögla, D.S. Su, Chem. Commun. 19 (2007) 1916–1918.
[15] J. Ji, X. Duan, G. Qian, P. Li, X. Zhou, D. Chen, W. Yuan, Catal. Today 216 (2013) 254–260.
[16] B.C. Gates, Chem. Rev. 95 (1995) 511–522.
[17] C.H. Chung, H.W. Yeom, B.D. Yu, I.W. Lyo, Phys. Rev. Lett. 97 (2006) 036103–36104.

[18] F.B. Mongeot, A. Toma, A. Molle, S. Lizzit, L. Petaccia, A. Baraldi, Phys. Rev. Lett. 97 (2006) 056103.
[19] C.B. Murray, D.J. Norris, M.G. Bawendi, J. Am. Chem. Soc. 115 (1993) 8706–8715.
[20] M. Bikshapathi, S. Singh, B. Bhaduri, G.N. Mathur, A. Sharma, N. Verma, Colloids Surf. A: Physicochem. Eng. Aspects 399 (2012) 46–55.
[21] Y. Jiang, K. Lin, Y. Zhang, J. Liu, G. Li, J. Sun, X. Xu, Appl. Catal. A: Gen. 445–446 (2012) 172–179.
[22] J.A. Arcibar-Orozco, J.R. Rangel-Mendez, T.J. Bandosz, J. Hazardous Mater. 246–247 (2013) 300–309.
[23] C. Popa, W.K. Offermans, R.A. van Santen, A.P.J. Jansen, Phys. Rev. B 74 (2006). 155428-10.
[24] G. Novell-Leruth, A. Valcárcel, J. Pérez-Ramírez, J.M. Ricart, J. Phys. Chem. C 111 (2007) 860–868.
[25] R.J. Lin, F.Y. Li, H.L. Chen, J. Phys. Chem. C 115 (2011) 521–528.
[26] S. Satoh, H. Fujimoto, H. Kobayashi, J. Phys. Chem. B 110 (2006) 4846–4852.
[27] J.C. Ganley, F.S. Thomas, E.G. Seebauer, R.I. Masel, Catal. Lett. 96 (2004) 117–122.
[28] J. Ji, X. Duan, X. Gong, G. Qian, X. Zhou, D. Chen, W. Yuan, Ind. Eng. Chem. Res. 52 (2013) 17151–17155.
[29] H.L. McKay, S.J. Jenkins, D.J. Wales, J. Phys. Chem. C 113 (2009) 15274–15287.
[30] S.C. Yeo, S.S. Han, H.M. Lee, J. Phys. Chem. C 118 (2014) 5309–5316.
[31] S.C. Yeo, Y.C. Lo, J. Li, H.M. Lee, J. Chem. Phys. 141 (2014). 134108-8.
[32] A.V. Postnikov, P. Entel, J.M. Soler, Eur. Phys. J. D 25 (2003) 261–270.
[33] E. Roduner, Chem. Soc. Rev. 35 (2006) 583–592.
[34] B. Pascucci, S. Otero, P.G. Belelli, F. Illas, M.M. Branda, J. Molec. Model. 20 (2014) 2448–2459.
[35] G. Lanzani, K. Laasonen, Int. J. Hydrogen Energy 35 (2010) 6571–6577.
[36] X. Zhang, Z. Lu, D. Ma, Z. Yang, Int. J. Hydrogen, Energy 40 (2015) 346–352.
[37] F.D. Kiss, R. Miotto, A.C. Ferraz, Nanotechnology 22 (2011) 275708.
[38] G. Kresse, J. Hafner, Phys. Rev. B 47 (1993) 558–561.
[39] G. Kresse, J. Hafner, Phys. Rev. B 48 (1993) 13115–13118.
[40] G. Kresse, J. Hafner, Phys. Rev. B 49 (1994) 14251–14268.
[41] P. Blochl, Phys. Rev. B 50 (1994) 17953–17979.
[42] J.P. Perdew, K. Burke, M. Ernzerhof, Phys. Rev. Lett. 77 (1996) 3865–3868.
[43] Z. Paál, P.G. Menon (Eds.), Hydrogen Effects in Catalysis: Fundamentals and Practical Applications, Marcel Dekker, New York, 1988. ISBN: 0-8247-7774-3.
[44] S. Grimme, J. Comput. Chem. 27 (2006) 1787–1799.
[45] H.J. Monkhorst, J.D. Pack, Phys. Rev. B 13 (1976) 5188–5192.
[46] J.J. Mortensen, M.V. Ganduglia-Pirovano, L.B. Hansen, B. Hammer, P. Stolze, J.K. Norskov, Surf. Sci. 422 (1999) 8–16.
[47] H. Jonsson, G. Mills, K.W. Jacobsen, Nudged Elastic Band Method for Finding Minimum Energy Paths of Transitions in Classical and Quantum Dynamics in Condensed Phase Simulations, in: B.J. Berne, G. Ciccotti, D.F. Coker (Eds.), World Scientific, Singapore, 1998, pp. 385–404. ISBN: 978-981-02-3498-0.
[48] P.E. Barnard, J.J. Terblans, H.C. Swart, Appl. Surf. Sci. 356 (2015) 213–220.
[49] R. Wu, A.J. Freeman, Phys. Rev. B 47 (1993) 3904.
[50] P. Błoński, A. Kiejna, Surf. Sci. 601 (2007) 123–133.
[51] C. Köhler, G. Seifert, T. Frauenheim, Comput. Mater. Sci. 35 (2006) 297–301.
[52] H.M. Duan, Q.Q. Zheng, Phys. Lett. A 280 (2001) 333–339.
[53] W.K. Offermans, A.P.J. Jansen, R.A. van Santen, G. Novell-Leruth, J.M. Ricart, J. Pérez-Ramírez, J. Phys. Chem. C 111 (2007) 17551–17557.
[54] Z. Jiang, Q. Pan, M. Li, T. Yan, T. Fang, Appl. Surf. Sci. 292 (2014) 494–499.
[55] Z. Jiang, P. Qin, T. Fang, Chem. Phys. 445 (2014) 59–67.
[56] X. Duan, G. Qian, C. Fan, Y. Zhu, X. Zhou, D. Chen, W. Yuan, Surf. Sci. 606 (2012) 549–553.
[57] W. Huang, C. Cheng, E. Feng, Surf. Sci. 616 (2013) 29–35.
[58] E. Sälli, V. Hänninen, L. Halonen, J. Phys. Chem. C 114 (2010) 4550–4556.
[59] K. Lejaeghere et al., Science 351 (6280) (2016). aad3000.
[60] W.G. Schmidt, K. Seino, M. Preuss, A. Hermann, F. Ortmann, F. Bechstedt, Appl. Phys. A 85 (2006) 387–397.
[61] G.S. Hammond, J. Am. Chem. Soc. 77 (1955) 334–338.
[62] J.E. Leffler, Science 117 (1953) 340–341.